Field Emission Patterns from First-Principles Electronic Structures: Application to Pristine and Cesium-Doped Carbon Nanotubes

Mohammad Khazaei,* Amir A. Farajian, and Yoshiyuki Kawazoe
Institute for Materials Research, Tohoku University, Sendai 980-8577, Japan
(Received 28 June 2005; published 21 October 2005)

A general approach is introduced to calculate field emission properties of any kind of nanostructure based on the first-principles local density of states (LDOS) and effective potentials. The experimental field emission spectroscopy images are explained as LDOS at the structure-vacuum barrier, weighted by the probability of electron tunneling. The method excellently reproduces the experimental field emission patterns of pristine capped carbon nanotubes. We show that cesium adsorbates even with a low doping ratio of one dopant per nanotube increase the emission current around 2.5 times, due to a generated dipole field.

DOI: 10.1103/PhysRevLett.95.177602 PACS numbers: 79.70.+q, 68.37.Vj, 73.22.−f, 85.45.Fd

Understanding the field emission process at the nanometer scale is essential in finding the best materials for long-lasting, low-threshold emission devices based on nanostructures [1–4]. The existing theoretical models for simulating the emission process include transfer matrix technique [5]; scattering formalism based on embedding potential [6]; integration of time-dependent Schrödinger equation [7]; classical statistical tunneling [8,9]; and perturbation theory, usually referred to as Bardeen transfer matrix method [10,11]. Penn and Plummer [12] use the last approach to propose a method for calculating field emission current from metallic surfaces when the momentum of emitting electrons parallel to the surface is small [13]. This assumption particularly applies to the case that at the length scale of the emitting structures, the surface is nonperiodic perpendicular to the emission direction.

We adapt the Penn-Plummer model to first-principles electronic structure calculations. Our approach is therefore quite general and can be applied to any kind of nanostructured surface including protrusion, impurity, and/or defects. Making use of the first-principles local density of states (LDOS) and effective potentials, our approach provides the ability to assess current emitted by individual electronic states at any point of nanostructure's surface. As an example of the applicability of our general method, we calculate field emission from pristine and Cs-doped capped nanotubes.

For capped nanotubes, the experimental images of Saito *et al.* [14] are explained as six bright pentagons with fivefold and sixfold symmetries, proposed to be the first direct observation of pentagon structures at the tip. Images obtained by Kuzumaki *et al.* [15] contain bright rings similar to a honeycomb. In both of these works, it is clearly observed that the centers of the bright rings and the boundary regions between them are dark. Field emission images of Dean *et al.* [16] show fivefold and sixfold symmetries of bright spots, explained as the spatially resolved cap states. Theoretically, Kim *et al.* [17] find that the charge density at the top of the armchair cap show two- or five-lobed patterns depending on the field strength. Buldum and Lu [18] show that at low applied electric field only apex atoms (the tip pentagon) emit; while by increasing the electric field more atoms start emitting. However, still the main features of field emission images are not clearly understood. Doped nanotubes emission is also under intensive study. The experiments carried out by Wadhawan *et al.* [19] show that the total emission current is significantly (up to 6 orders of magnitude) increased after Cs deposition. However, experiments of Kim *et al.* [20] show an increase of 1 order of magnitude.

In first-principles electronic structure calculations, the supercell is generally discretized by introducing a fine grid. This grid divides the supercell face perpendicular to the emission direction into small surface elements. In order to calculate field emission current j of a nanostructure, we need to calculate the emission current along individual grid lines parallel to the emission direction. Thus, the total current emitted by the electronic state with energy ω is calculated to be the sum of the currents along the grid lines i: $j(\omega) = \sum_i j_i(\omega)$. The currents $j_i(\omega)$ are expressed as [12]

$$j_i(\omega) = \frac{2e\hbar}{m_e} f(\omega) S_i \lambda_i^{-2}(\omega) D_i^2(\omega) g_i(\omega, x_{l,i}). \quad (1)$$

In Eq. (1), m_e is the electron effective mass, $f(\omega)$ is the Fermi-Dirac distribution, and S_i is the area of the surface element i. $\lambda_i(\omega)$ is a slowly varying function of energy resulting from the asymptotic matching of the wave function of emitting state at the left turning point $x_{l,i}$ with WKB wave function inside the barrier. The left and right turning points, $x_{l,i}$ and $x_{r,i}$, along the grid line i are determined as the points where the energy of the emitting state becomes equal with the potential energy barrier $u_i(x)$, with x being the coordinate along the emission direction. $D_i^2(\omega)$ indicates the probability of electron tunneling through the nanostructure-vacuum barrier $u_i(x)$, and $g_i(\omega, x_{l,i})$ is the

LDOS at the left turning point. $\lambda_i(\omega)$ is given by

$$\lambda_i(\omega) = (\pi/3)^{1/2}(c_i/3)^{-1/3}\left[\Gamma\left(\frac{2}{3}\right)\cos(\pi/6)\right]^{-1}, \quad (2)$$

where c_i is obtained by fitting $(2m_e/\hbar^2)(u_i(x) - \omega)$ to $c_i^2(x - x_{l,i})$ at the left turning point. The tunneling probability $D_i^2(\omega)$ is expressed as

$$D_i^2(\omega) = \exp\left[-2\sqrt{\frac{2m_e}{\hbar^2}}\int_{x_{l,i}}^{x_{r,i}}\sqrt{u_i(x) - \omega}\,dx\right]. \quad (3)$$

Within our approach, the necessary data for calculating emission currents $j_i(\omega)$, i.e., LDOS $g_i(\omega, x_{l,i})$ and the potential energy $u_i(x)$, are obtained from first-principles calculations. The probability $D_i^2(\omega)$ along each grid line is calculated by numerical integration.

The introduced model is applied to pristine and Cs-doped capped nanotubes to explain the recent experimental results [14–16,19,20]. Our pristine capped nanotube structure consists of 290 carbon atoms. The cap is represented by half of C_{240} fullerene and the stem is constructed from (10,10) armchair nanotube. We also consider two different Cs-doped capped nanotube structures. The doped structures are formed by adsorbing/trapping the Cs atom at the cap, as depicted in Fig. 1. The structure with adsorbed Cs, Fig. 1(a), resembles a minimally deformed doped nanotube, while the structure with the Cs trapped at the tip, Fig. 1(b), is formed by detachment of the tip pentagon [21]. Our first-principles calculations are performed using SIESTA code [22–24]. Details of settings and their justifications are explained in Refs. [21,25]. The capped structures are relaxed while keeping two ending carbon rings at the open end fixed. The ending C-C bond lengths are reduced to 1.24 Å.

Figure 2 describes our model for calculating field emission current of pristine capped (10,10) nanotube. Figure 2(a) shows the first-principles effective potential $u_i(x)$ along the nanotube axis, under electric fields 0.07, 0.3, and 0.5 V/Å. It is observed that the effective potential height, and the energy of the highest occupied molecular orbital (HOMO) are changed under different electric fields [26]. Therefore the capped nanotubes cannot be simulated like a perfect metallic hemisphere [8,9] with a fixed potential height. Upon finding the left and right turning points, $x_{l,i}$ and $x_{r,i}$, the LDOS at the left turning points, $g_i(\omega_{\mathrm{HOMO}}, x_{l,i})$, and the tunneling probability, $D_i^2(\omega_{\mathrm{HOMO}})$, are calculated. Figure 2(b) shows the HOMO LDOS along the nanotube axis for various electric fields. In Fig. 2(c) the HOMO LDOS is zoomed in to show the proximity of the left turning points $x_{l,i}$, indicated by arrows. By calculating the HOMO tunneling probability for grid lines other than the nanotube's axis, the HOMO tunneling probability pattern is derived. Figure 2(d) shows the pattern under electric field 0.3 V/Å. It is observed that the tunneling probability from the tip pentagon is more than that from other cap points. Having obtained the tunneling probability and using the variation of the effective potential near $x_{l,i}$, we calculate $\lambda_i(\omega)$ and the emission current $j_i(\omega)$ for all the grid lines i and energies ω of the emitting states. The energies of the emitting states are restricted by the tunneling probabilities and the Fermi-Dirac distribution.

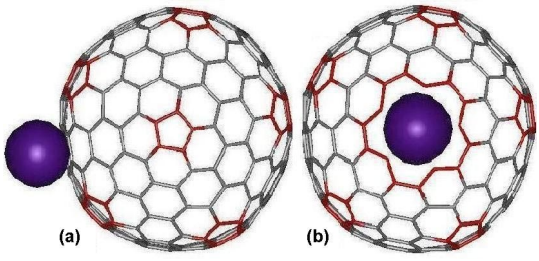

FIG. 1 (color online). Two typical Cs-doped capped (10,10) nanotube structures: Cs adsorbed at the cap (a) and Cs trapped at the tip (b). The nanotube axis is perpendicular to the page.

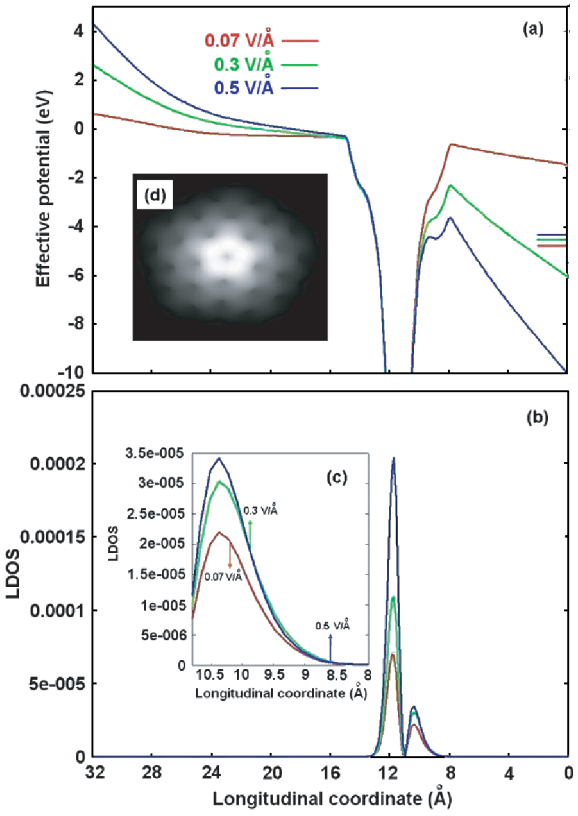

FIG. 2 (color). Variation of the effective potential $u_i(x)$ (a), and HOMO LDOS $g_i(\omega_{\mathrm{HOMO}}, x)$ (b) along the nanotube axis of the pristine capped (10,10) nanotube, under different electric fields. The LDOS curves near the left turning points x_l, indicated by arrows, are zoomed in (c). HOMO energies are indicated by colored ticks of the right axis in (a). The pattern of HOMO tunneling probability, $D^2(\omega_{\mathrm{HOMO}})$, under electric field 0.3 V/Å is depicted in (d). The tip pentagon of the cap and the ending carbon ring of the open end of the stem are located at 11.6 and 28.7 Å, respectively.

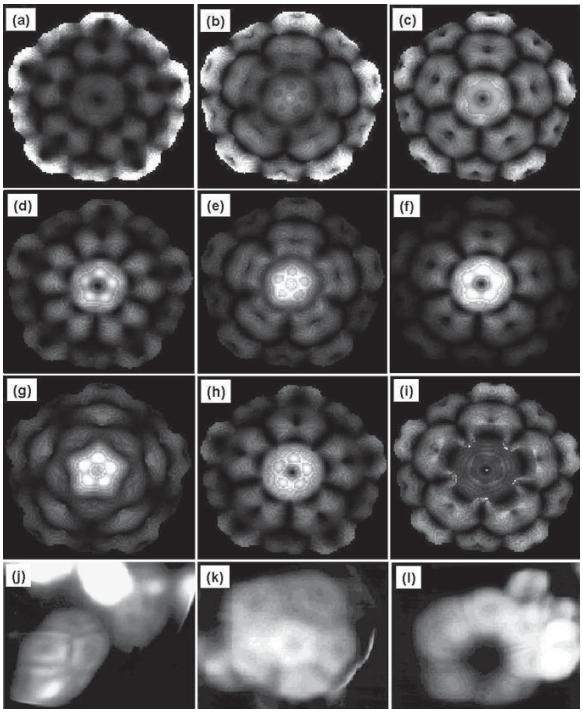

FIG. 3. The LDOS patterns at the left turning points for the pristine capped (10,10) nanotube's emitting states: (HOMO − 1) + (HOMO − 2) (a), HOMO + LUMO (b), and (LUMO + 1) + (LUMO + 2) (c) under electric field 0.3 V/Å. The corresponding current emission patterns are depicted in (d), (e), and (f), respectively. The current patterns under electric field 0.5 V/Å are shown for (HOMO − 3) + (HOMO − 4) + (HOMO − 5) + (HOMO − 6), (HOMO − 1) + (HOMO − 2) and HOMO + LUMO + (LUMO + 1) + (LUMO + 2) in (g), (h), and (i). The same brightness indicates different values in different figures (cf. Table I). The experimental results of Kuzumaki *et al.* [15] (j) and Saito *et al.* [14] (k), (l) are also shown.

Figures 3(a)–3(c) show the calculated patterns of LDOS at the left turning points, under the electric field 0.3 V/Å, for different emitting states. The corresponding current emission patterns are shown in Figs. 3(d)–3(f). In these figures, the effects of nearly degenerate states are combined. Table I shows the energy-resolved current emission under electric field 0.3 V/Å for the three topmost emitting states. For this particular system, the λ function has nearly the same value at all the surface grid points, for each particular energy. Hence, the emission current patterns are mainly determined by the tunneling probability D_i^2 and LDOS $g_i(x_{l,i})$ as observed, e.g., by comparing the current emission pattern of Fig. 3(e) with the LDOS of Fig. 3(b) and the tunneling probability of Fig. 2(d). The emission current patterns under the electric field 0.5 V/Å are shown in Figs. 3(g)–3(i). The total emission current in this case is 30 times larger than the total current under 0.3 V/Å. Our obtained emission current patterns excellently reproduce the observed features of the experimental patterns of Refs. [14–16]: The bright hexagons that encircle the central bright pentagon in Figs. 3(e), 3(f), and 3(h) have dark centers and dark straight boundaries. Their side views resemble the features of the experimental pattern of Fig. 3(j), although the experimental structure may differ from that of ours. The similarities are more remarkable for Figs. 3(k) and 3(l): Figs. 3(f) and 3(h) both have the central bright pentagon with dark center and the surrounding five bright hexagons with dark centers that are observed in Fig. 3(k). Moreover, the experimental pattern of Fig. 3(l), with its dark center and surrounding bright hexagons, is clearly reproduced in Fig. 3(i). The last feature indicates the penetration of strong electric fields into the cap [27], as a result of field enhancement at the tip. Even under the same applied field the enhancement factor can be different for different emitting nanotubes, due to diverse local aspect ratios in experiments. The relative intensity of emission from different states is also affected by the local temperature (taken to be 300 K in our

TABLE I. Energy-resolved current emission from different energy levels of pristine capped (10,10) nanotubes under electric field 0.3 V/Å. The total emission current is 5.0 μA.

Energy levels	Emission current (μA)
(HOMO − 1) + (HOMO − 2)	0.2
HOMO + LUMO	0.5
(LUMO + 1) + (LUMO + 2)	0.1

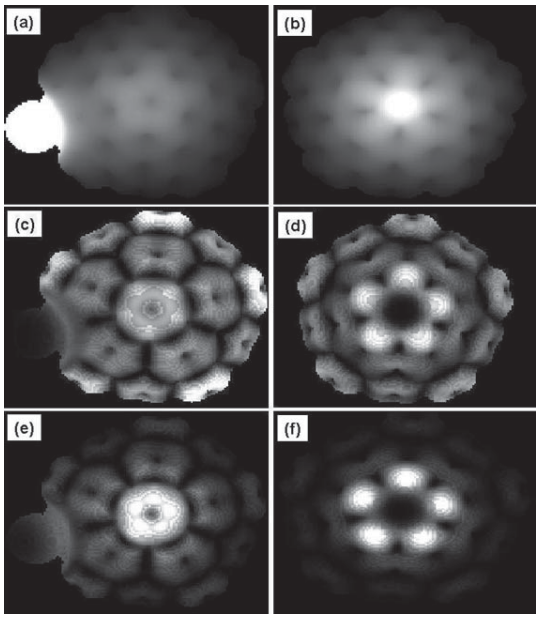

FIG. 4. The tunneling probability patterns for the Cs adsorbed (a) and trapped (b) at the capped (10,10) nanotube, under the electric field 0.3 V/Å from the energy levels (HOMO − 1) + (HOMO) + (LUMO) + (LUMO + 1). The corresponding LDOS at the left turning points are depicted in (c) and (d). (e) and (f) represent the current emission patterns.

TABLE II. Current emission from pristine and Cs-doped capped (10,10) structures under the electric field 0.3 V/Å.

Structure	Total emission current (μA)
Pristine nanotube	5.0
Cs adsorbed at the cap	13.4
Cs trapped at the tip	12.5

calculations). Hence the calculated patterns of various emitting states will resemble the experimental patterns, if the aspect ratio and local temperature of the emitting nanotube result in the corresponding local electric field and occupation of states.

Figures 4(a) and 4(b) show the tunneling probability patterns of the two Cs-doped structures shown in Figs. 1(a) and 1(b), respectively. The energy levels HOMO-1, HOMO, lowest unoccupied molecular orbital (LUMO), and LUMO + 1 are nearly degenerate and are combined together. The corresponding LDOS patterns are depicted in Figs. 4(c) and 4(d), while the current emission patterns are shown in Figs. 4(e) and 4(f). As seen from Figs. 4(a) and 4(b), the tunneling probability from the Cs and connecting carbon atoms is more than that from other atomic sites. This can be explained by Cs ionization at carbon lattice, remarkably seen, e.g., from the similarity of Figs. 3(c) and 4(c): The created dipole field causes the height of the effective potential around the Cs sites to decrease, and the corresponding tunneling probability to increase. One may expect that current emission should also reach maximum at the Cs sites, as they constitute sharp points at the cap. However, Figs. 4(c) and 4(d) show that there are no localized electrons on the Cs sites at the left turning points. This is the reason that no current emission is observed from the Cs sites in field emission patterns of Figs. 4(e) and 4(f). It indicates the significant importance of separating the roles of tunneling probability and local density of states in interpreting the emission process. Figure 4(d) shows that most of the states near HOMO level are localized at the unsaturated bonds created by the detachment of the tip pentagon. Combined with the high tunneling probability of the Cs site and its surroundings, this causes the current emission to peak at these atomic sites, as observed in Fig. 4(f). Table II shows the total emission currents. The results are obtained for $m_e = 0.175 m_0$ [28] where m_0 is free electron mass. If $m_e = m_0$, the total currents are around 100 (for doped structures) to 1000 (for pristine structure) times smaller. We see that after Cs doping, with one Cs per emitting nanotube, the current emission increases around 2.5 times, independent of the details of the adsorption site. Higher doping levels would result in further increase of the emission current. Our results therefore support experimental observations of Kim *et al.* [20]. The difference with Wadhawan *et al.* experiments [19] might be explained by the difference of the Cs deposition density [29], or different field enhancement factors.

To conclude, we introduce a theoretical method for calculating nanometer-scale field emission based on first-principles electronic structures. The emission pattern has the resolution of the first-principles supercell grid. The roles of tunneling probability and local density of states in current emission is separated and clarified. The application of the method to the case of pristine and cesium-doped nanotubes is shown to agree excellently with the experimental emission results.

*Electronic address: khazaei@imr.edu

[1] Y. B. Tang *et al.*, Appl. Phys. Lett. **86**, 153104 (2005).
[2] K. Yu *et al.*, Mater. Lett. **59**, 1866 (2005).
[3] T. Sugino *et al.*, Diam. Relat. Mater. **12**, 464 (2003).
[4] Y. Huh *et al.*, Thin Solid Films **475**, 267 (2005).
[5] A. Mayer *et al.*, J. Phys. Condens. Matter **15**, R177 (2003).
[6] H. Ishida, D. Wortmann, and T. Ohwaki, Phys. Rev. B **70**, 085409 (2004).
[7] S. Han and J. Ihm, Phys. Rev. B **66**, 241402(R) (2002).
[8] V. Filip *et al.*, J. Vac. Sci. Technol. B **21**, 382 (2003).
[9] G. Zhou, W. Duan, and B. Gu, J. Chem. Phys. **121**, 12 600 (2004).
[10] J. Bardeen, Phys. Rev. Lett. **6**, 57 (1961).
[11] H. Reittu, Am. J. Phys. **63**, 940 (1995).
[12] D. R. Penn and E. W. Plummer, Phys. Rev. B **9**, 1216 (1974); D. R. Penn, Phys. Rev. B **14**, 849 (1976).
[13] The effects of surface periodicity are addressed by R. Ramprasad, L. R. C. Fonseca, and P. von Allmen, Phys. Rev. B **62**, 5216 (2000).
[14] Y. Saito, K. Hata, and T. Murata, Jpn. J. Appl. Phys. **39**, L271 (2000).
[15] T. Kuzumaki *et al.*, Diam. Relat. Mater. **13**, 1907 (2004).
[16] K. A. Dean and B. R. Chalamala, J. Appl. Phys. **85**, 3832 (1999).
[17] C. Kim *et al.*, Appl. Phys. Lett. **79**, 1187 (2001).
[18] A. Buldum and J. P. Lu, Phys. Rev. Lett. **91**, 236801 (2003).
[19] A. Wadhawan, R. E. Stallcup II, and J. M. Perez, Appl. Phys. Lett. **78**, 108 (2001).
[20] D.-H. Kim *et al.*, Chem. Phys. Lett. **355**, 53 (2002).
[21] M. Khazaei *et al.*, J. Phys. Chem. B **108**, 15 529 (2004).
[22] P. Ordejón, E. Artacho, and J. M. Soler, Phys. Rev. B **53**, R10441 (1996).
[23] J. M. Soler *et al.*, J. Phys. Condens. Matter **14**, 2745 (2002).
[24] D. Sánchez-Portal *et al.*, J. Phys. Condens. Matter **8**, 3859 (1996).
[25] M. Khazaei *et al.*, Comput. Mater. Sci. (to be published).
[26] See also C.-W. Chen, M.-H. Lee, and S. J. Clark, Diam. Relat. Mater. **13**, 1306 (2004).
[27] X. Zheng *et al.*, Phys. Rev. Lett. **92**, 106803 (2004).
[28] A. Jorio *et al.*, Phys. Rev. B **71**, 075401 (2005).
[29] E. P. Gyftopoulos and J. D. Levine, J. Appl. Phys. **33**, 67 (1962).